Spherical harmonics analysis of *Fermi* gamma-ray data and the Galactic dark matter halo

Dmitry Malyshev,* Jo Bovy,† and Ilias Cholis‡

Center for Cosmology and Particle Physics
4 Washington Place, Meyer Hall of Physics,
NYU, New York, NY 10003

We argue that the decomposition of gamma-ray maps in spherical harmonics is a sensitive tool to study dark matter (DM) annihilation or decay in the main Galactic halo of the Milky Way. Using the spherical harmonic decomposition in a window excluding the Galactic plane, we show for one year of *Fermi* data that adding a spherical template (such as a line-of-sight DM annihilation profile) to an astrophysical background significantly reduces χ^2 of the fit to the data. In some energy bins the significance of this "DM" fraction is above three sigma. This can be viewed as a hint of DM annihilation signal, although astrophysical sources cannot be ruled out at this moment. We use the derived "DM" fraction as a conservative upper limit on DM annihilation signal. In the case of $b\bar{b}$ annihilation channel the limits are about a factor of two less constraining than the limits from dwarf galaxies. The uncertainty of our method is dominated by systematics related to modeling the astrophysical background. We show that with 1 year of *Fermi* data the statistical sensitivity would be sufficient to detect DM annihilation with thermal freeze out cross section for masses below 100 GeV.

PACS numbers: 95.85.Pw, 95.55.Ka, 98.70.Rz, 95.35.+d

I. MOTIVATION

Out of all indirect searches for dark matter (DM), gamma-rays are probably the most "direct" [1, 2]. Charged particles, such as positrons and antiprotons, are deflected in the Galactic magnetic field. The information about their source is lost and only anomalies in the spectrum may signal about the presence of DM. Most of gamma-rays propagate freely inside the Galaxy and, together with the spectrum, they carry information about the morphology of the source. This property may be crucial in separating a DM signal from astrophysical backgrounds, e.g., [3].

From cosmological simulations [4–7], we expect that cold dark matter in our Galaxy has formed a nearly spherical halo with density growing towards the Galactic center (GC). Thus, DM annihilation or decay may be a source of gamma-rays with a spherical shape peaked at the GC, in addition to astrophysical and extra-galactic sources.

In this paper, we study the contribution from the main spherical halo ignoring DM substructure. In order to minimize the astrophysical flux, we mask the Galactic plane and resolved gamma-ray point sources. The problem is that at high latitudes a possible DM annihilation signal is relatively smooth and most probably subdominant to Galactic and extragalactic diffuse emission. In the paper we propose to use the spherical harmonics decomposition of gamma-ray data to search for DM annihilation or decay. The contribution of a smooth signal with small amplitude is maximal for spherical harmonics with small angular numbers ℓ. Consequently, the Galactic DM signal away from the GC may contribute most significantly to small ℓ harmonics, while its contribution to large ℓ harmonics can be neglected compared to the Poisson noise.

Spherical harmonics decomposition has several advantages compared to template fitting in coordinate space:

1. **Organization of data:** small ℓ harmonics carry all the information about the large scale distribution of sources, while large ℓ harmonics are dominated by the Poisson noise. Spherical harmonics decomposition is a linear transformation that has no information loss, but only relevant information for large scale distributions is used in fitting.

2. **Universality:** small ℓ harmonics are insensitive to the resolution of pixel maps (for sufficiently small pixel sizes). In particular, the templates may have different resolution and don't need to be brought to the same pixel size as in the case of coordinate space fitting. The χ^2 is also independent of resolution, while in coordinate space the absolute likelihood depends on the number of pixels.

3. **Linearity and stability:** both the transformation of data from coordinate space and the fitting in spherical harmonics space are linear operations (the χ^2 has the usual quadratic form). Thus, a nonlinear Poisson likelihood in coordinate space is substituted by a combination of two linear operations

in spherical harmonics space. This may be useful for stability of fitting procedure in the case of small numbers of photons in pixels: the Poisson probability is undefined for non-positive expected number of photons, while small negative expected numbers should not a be problem, it simply means that the template is not perfect and we over-subtract this template to fit data somewhere else.

4. **Symmetry:** in some cases spherical harmonics may be useful to focus on a part of data with a particular symmetry in mind. In this paper we will use the spherical symmetry of dark matter distribution around the Galactic center. If we point the z-axis towards the GC, then dark matter contributes only to Y_{lm} harmonics with $m = 0$, i.e., we may select only a_{l0} modes in fitting.

A computational algorithm for fitting in spherical harmonics space is straightforward but there are a few things to keep in mind. Firstly, the Y_{lm}'s are not orthogonal in a window on the sphere. The corresponding spherical modes a_{lm}'s are still independent but correlated. As a result, their covariance matrix is not diagonal. In general, this may render the computations unfeasible, unless one uses some special techniques (such as the Gabor transform for the power spectrum [8]). We will use only a few Y_{l0} harmonics corresponding to the largest scales. The corresponding covariance matrix is relatively small and can be easily computed.

The choice of the astrophysical background model is a more conceptual problem. A thorough solution of this problem can be quite complicated and we will not discuss it here. The main purpose of our work will be to illustrate the method of the spherical harmonics transform in the analysis of gamma-rays. As a toy model for the astrophysical background we will use the gamma-ray distribution in a low energy bin, since we expect that the DM contribution to the spectrum is insignificant at low energies.

The paper is organized as follows. In Section II we describe an algorithm of fitting templates in spherical harmonics space. In Section III we apply this method for *Fermi* gamma-ray data. We compare two cases. In the first case we use two templates: a low energy bin and an isotropic distribution. In the second case we also add a distribution of photons with a spherical symmetry around GC. We find that the residual for the three-template models has a much better χ^2 than the residual for the two-template model. In Section IV we find the best fit energy spectrum of the fluxes assuming a power-law dependence on energy. We also put constraints on DM annihilation in $b\bar{b}$. Section V has conclusions.

There are three appendices. In Appendix A we calculate the covariance matrix for spherical harmonics defined on a window in the sphere. In Appendix B we check the fitting algorithm with a Monte Carlo simulation. In Appendix C we discuss the contribution to the angular power spectrum from point sources.

II. METHOD

In this section we describe a general method of template fitting in spherical harmonics space. In the next section we apply this method to the *Fermi* gamma-ray data to search for DM annihilation in the Milky Way halo.

In general, an algorithm will contain several steps:

1. Choose a mask (for instance, one can mask the Galactic plane and point sources).

2. Find the spherical harmonics decomposition of the data outside of the masked region, a_{lm}.

3. Find the covariance matrix for the spherical harmonics coefficients, $\mathrm{Cov}(a_{lm}, a_{l'm'})$.

4. Formulate a model for the gamma-ray distribution as a function of parameters α and find the corresponding decomposition into spherical modes $b_{lm}(\alpha)$ outside of the mask.

5. Find the best fit model parameters α_* by minimizing a χ^2 where we use the full covariance matrix instead of σ^2 due to a non-trivial correlation of the spherical modes on a window in the sphere (Equation (A5)).

In the remaining part we will mostly introduce the notations that will be necessary in interpreting the results of data analysis in the next section. The mathematical details can be found in Appendix A.

In the calculations of spherical harmonics decomposition, it is convenient to use a pixelation of the sphere (we use HEALpix [9]). We will consider some energy bins E_i and denote by $n_p(E_i)$ the number of photons inside the energy bin i in a pixel $p = 1, \ldots, N_{\mathrm{pix}}$. For clarity, in the following formulas we will suppress the dependence on energy.

Define the photon density as $\rho(\gamma_p) = \frac{n_p}{\delta\Omega_p}$, where $\delta\Omega_p$ is the size and γ_p is the center of the pixel p. We put $n_p = \rho(\gamma_p) = 0$, if the center of the pixel is inside the mask. The spherical harmonics transform of the gamma-ray data is

$$a_{lm} = \int Y_{lm}^*(\gamma)\rho(\gamma)d\Omega \approx \sum_{p=1}^{N_{\mathrm{pix}}} Y_{lm}^*(\gamma_p)n_p. \qquad (1)$$

In Appendix A we show that the covariance matrix has the following simple expression

$$\mathrm{Cov}(a_{lm}, a_{l'm'}) = \sum_p Y_{l'm'}^*(\gamma_p)Y_{lm}(\gamma_p)n_p. \qquad (2)$$

Let us now describe the parameterization of the models. In general, the shape of the model fluxes can depend on some parameters. In this paper we will focus on the template fitting, where the shape of the templates for

various sources is fixed and the only variable parameters are the normalizations in every energy bin.

For each template α in every energy bin, the variable parameter will be the average flux inside the window F^α in units of $\frac{1}{\text{GeV cm}^2\,\text{s sr}}$. In order to find the number of photons in a pixel p from a template α, one needs to multiply F^α by the *Fermi* exposure E_p times the probability distribution function (PDF) ρ_p^α that carries the information about the shape of the template α, times the size of the window Ω_W, times the size of the energy bin ΔE. The number of photons from the template α in a pixel p is

$$n_p^\alpha = F^\alpha \cdot (E_p \cdot \rho_p^\alpha \cdot \Omega_W \cdot \Delta E), \qquad (3)$$

where the PDF is normalized as $\sum_p \rho_p^\alpha = 1$. Let us denote the spherical harmonics decomposition of the function in the parenthesis as

$$v_{lm}^\alpha = \sum_{p=1}^{N_{\text{pix}}} Y_{lm}^*(\gamma_p)(E_p \cdot \rho_p^\alpha \cdot \Omega_W \cdot \Delta E), \qquad (4)$$

then the spherical harmonics decomposition of a linear sum of sources is

$$b_{lm}(F^\alpha) = \sum_\alpha F^\alpha v_{lm}^\alpha \qquad (5)$$

The best fit fluxes F_*^α can be found from minimizing the χ^2 in Equation (A5).

The uncertainty of the model parameters F^α around the minimum of χ^2 can be estimated from the Hessian matrix

$$H_{\alpha\beta} = \left. \frac{\partial^2 \chi^2}{\partial F^\alpha \partial F^\beta} \right|_{F^\alpha = F_*^\alpha}. \qquad (6)$$

In particular, the variance of the model fluxes can be estimated as

$$\text{Var}(F^\alpha) = H^{-1}{}_{\alpha\alpha}. \qquad (7)$$

III. DATA ANALYSIS

A. Data selection

We consider 13 months of *Fermi* gamma-ray data (August 4, 2008 till August 25, 2009) that belong to the "diffuse class" (Class 3) of the LAT pipeline. We exclude the data beyond zenith angles of 105° due to significant contamination from atmospheric gamma-rays. We also exclude the data taken over the South Atlantic Anomaly (SAA) and mask the point sources detected by *Fermi* [10].

Most of the time we will use the gamma-rays between 1 GeV and 300 GeV which we separate in 10 exponential energy bins between 1 GeV and 100 GeV plus an extra energy bin between 100 GeV and 300 GeV. We mask

the pixels centered within 10° from the Galactic plane. We also mask all pixels that either contain a gamma-ray point source or if the boundary of the pixel is within 68% containment angle $\approx 0.7°$ at $E = 1$ GeV [11] to a gamma-ray point source.

The interpretation of spherical harmonics decomposition of a DM model is simplest in the coordinate system where the z-axis points towards the GC (at odds with the standard Galactic coordinates in which the z-axis points towards the Galactic North pole). We choose the x-axis pointing towards the Galactic South pole. If we were considering all data without masking, then DM would contribute only to Y_{l0} harmonics due to a rotational symmetry round the new z-axis. In the presence of a mask, DM contributes to all spherical harmonics, but its contribution to Y_{l0} modes is still maximal and we will restrict our attention to these modes for simplicity of analysis.

Pixelation of the data and spherical harmonics decomposition is performed with *healpy*, the python version of HEALPix [9][34].

An example of gamma-ray counts map for the energy bin between 1 GeV and 1.6 GeV with the z-axis pointing towards the GC can be found in Figure 1.

Summary of data selection and model parameters:

1. Mask the gamma-ray point sources and the Galactic plane within $|b| < 10°$;

2. Rotate the z-axis to point towards the GC;

3. Consider Y_{lm} harmonics with $\ell \leq 15$ and $m = 0$;

4. We choose HEALPix parameter nside = 32 (corresponding to pixel size of about 2°);

5. Astrophysics template energy bin: 1 GeV < E < 1.6 GeV.

These are the data selection parameters for the "main" example that we consider in Section III B. In Section III C we consider the effect of varying these parameters.

B. Bin to bin fitting

We use the energy bin between 1 GeV and 1.6 GeV as a template for the Galactic astrophysical emission assuming that the gamma-ray emission at these energies is dominated by the Galactic cosmic ray production through the π^0 decay. One of the possible limitations of this template is the inverse Compton scattering (ICS) component of gamma-rays. Relative contribution from the ICS photons increases with energy and may become comparable to π^0 photons above 10 GeV [12]. As a result, a low energy bin template may underestimate the ICS component at higher energies. Currently, there is no generally accepted model for the ICS emision (see, e.g., the caveats section in the description of the *Fermi* diffuse background model [35]). We will treat the ICS component as a systematic uncertainty in the current analysis.
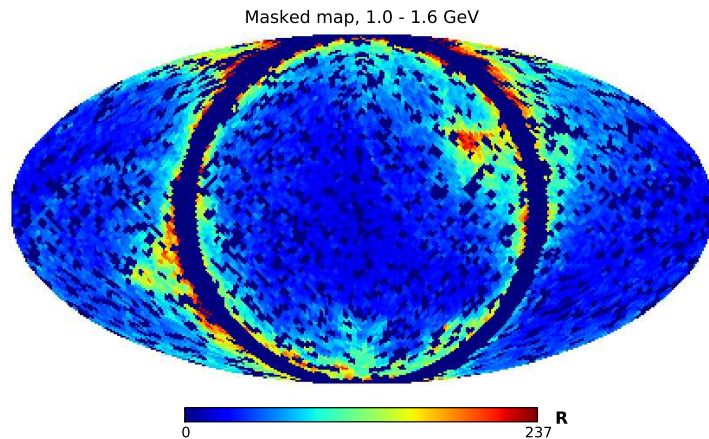
FIG. 1: Counts in pixels for 1 - 1.6 GeV energy bin. The Galactic center is in the North pole, the anti-center is in the South pole (Southern hemisphere is in the center). We mask $|b| < 10°$ and gamma-ray point sources detected by *Fermi* [10].
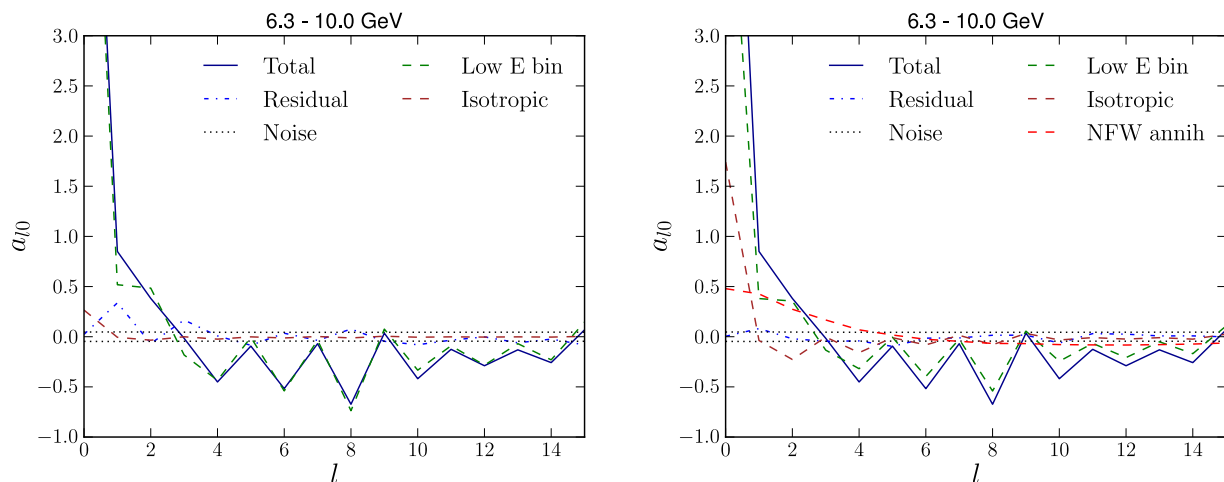

FIG. 2: An example of the a_{lm} fitting procedure for $m = 0$ and $\ell = 0, \ldots, 15$ in the 6.3 GeV to 10 GeV energy bin. The harmonic decomposition in a window is defined in Section II (there is an additional HEALPix normalization factor $4\pi/N_{\text{pix}}$ with respect to Equation (1)). The low energy bin a_{lm}'s are given by the gamma-ray data in 1 GeV to 1.6 GeV energy bin. The isotropic template a_{lm}'s are non-zero for $\ell > 0$ due to the spherical harmonics decomposition in a window. Large fluctuations of data a_{lm}'s are mostly due to symmetry of the mask and the fact that the Galactic flux is stronger near the Galactic plane (notice, that the modes with even ℓ are significantly larger than the modes with odd ℓ's). The noise level is given by the square root of the diagonal elements in the covariance matrix in Equation (2). The χ^2 for the two-template fit on the left is 80 for 14 dof, while the three-template fit on the right has $\chi^2 = 16$ for 13 dof. The χ^2 in other energy bins can be found in Section III D where we also compare the NFW annihilation profile with other profiles.

We consider an isotropic template as a model for the extragalactic emission. We will also consider several templates with a spherical distribution around the GC. Our main working example will be the line-of-site DM annihilation in Navarro, Frenk, and White (NFW) profile [4]. The NFW profile is

$$\rho_{\text{DM}}(r) \propto \frac{r}{r_s} \frac{1}{(1 + r/r_s)^2} \qquad (8)$$

where the scale parameter $r_s = 20$ kpc [13, 14]. The window angle $|b| > 10°$ corresponds to distances $r > 1.5$ kpc from the GC. At these distances the NFW profile is

similar to less cuspy profiles, such as the Einasto profile [15]. The annihilation signal is proportional to ρ_{DM}^2, cf., Equation 16.

As a null hypothesis we take a combination of two templates: an astrophysical template modeled by a low energy bin and an isotropic flux. We compare this model with the three template model, where we also add a template with spherical symmetry around the GC. In fitting, we decompose the templates and the data in every energy bin into spherical harmonics according to the algorithm in Section II. The fluxes corresponding to the templates are found by minimizing the χ^2 in Equation (A5). An
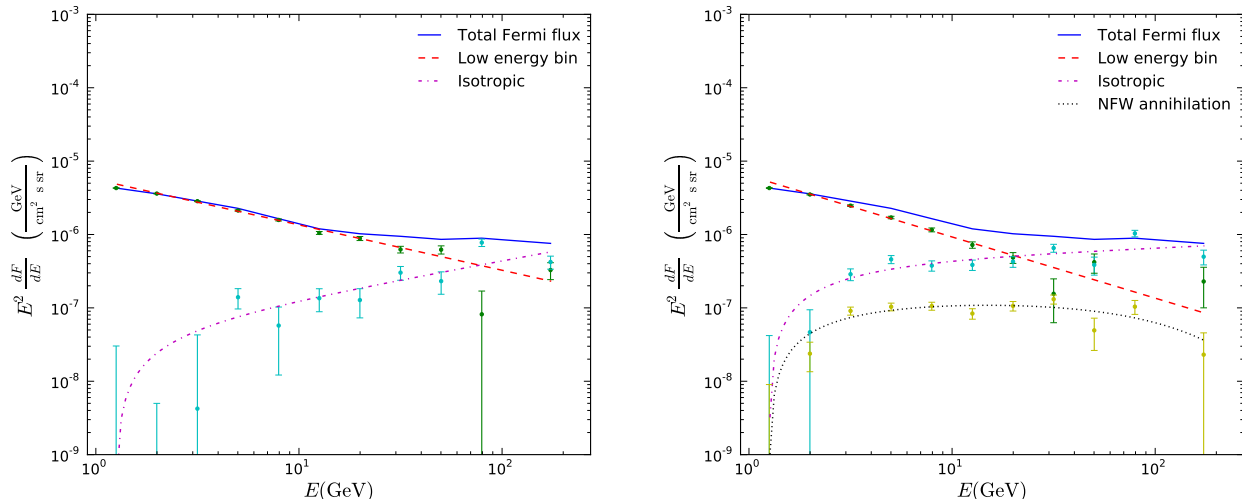
FIG. 3: Left plot: two-template model fitting. Right plot: three-template model fitting. Points represent fitting in every energy bin independently. Lines represent best fit with power-law spectra discussed later in Section IV. The first bin is "singular" since we use the data in this bin as one of the templates. The points associated with NFW annihilation template are significantly above zero, i.e., there is a significant signal that grows towards the GC, but, as we show in Figure 6, other profiles with rotational symmetry around GC give similar improvement of χ^2, i.e., current data are not sufficient to distinguish different profiles and understand the nature of the signal. In Section IV B we will use the points associated with NFW annihilation profile to put conservative upper limits on annihilation cross-section.

example of fitting the data in an energy bin between 6.3 and 10 GeV using the spherical harmonics is presented in Figure 2. The results of fitting in every energy bin are shown in Figure 3.

The best fit value of the flux corresponding to the spherical template can be used to put a conservative upper bound on DM annihilation into a pair of monochromatic photons (the DM line signal). The upper bounds obtained this way are an order of magnitude less constraining than the limits on monochromatic gamma-rays obtained by *Fermi* collaboration [16]. Spherical harmonics decomposition method has a better performance for signals with smooth energy dependence. In Section IV B we find conservative limits on $b\bar{b}$ DM annihilation only a factor of a few less constraining than the limits from dwarf spheroidal galaxies [17].

C. Variation of parameters

In this subsection we check the robustness of spherical harmonics decomposition with respect to variation of data selection and model parameters. The main model is given by the flux associated with NFW annihilation template found in Section III B with parameters defined in Section III A. We consider the following variations of parameters (Figure 4):

1. Different energy bins for the astrophysics template: 0.7 GeV $< E <$ 1 GeV and 2.5 GeV $< E <$ 4 GeV. The contribution above 10 GeV is consistent with the main model.
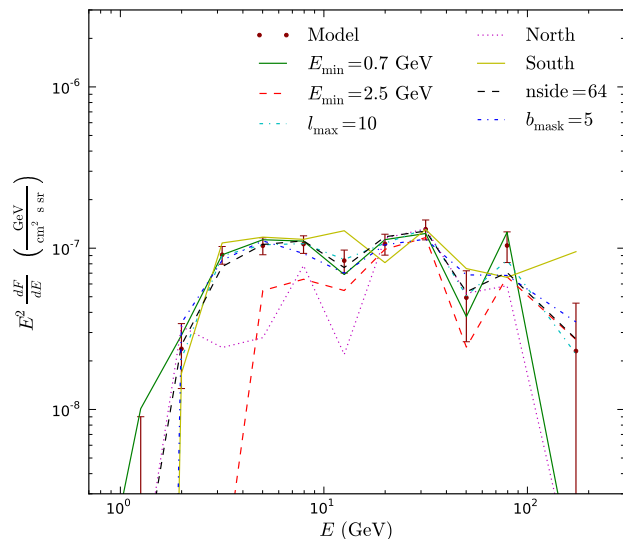

FIG. 4: Dependence of flux associated with NFW annihilation template on model parameters. The main model and the variations are described in Sections III B and III C.

2. The DM flux does not change significantly if we shrink the window size to $|b| < 5°$, change the number of harmonics to $\ell_{\max} = 10$, or change the resolution to nside = 64 (pixel size of about 1°).

3. Separating the Northern and the Southern hemispheres: the contribution of the spherical template

in the North is significantly smaller than in the South. This may be due to a stronger astrophysical flux in the North (compare with the SFD dust template that is believed to trace the π^0 production of gamma-rays [18, 19]).

We performed other variations, such as increasing the window size and increasing $\ell_{\max}$ (not shown in Figure 4). We find that the variation of parameters doesn't change the results significantly.

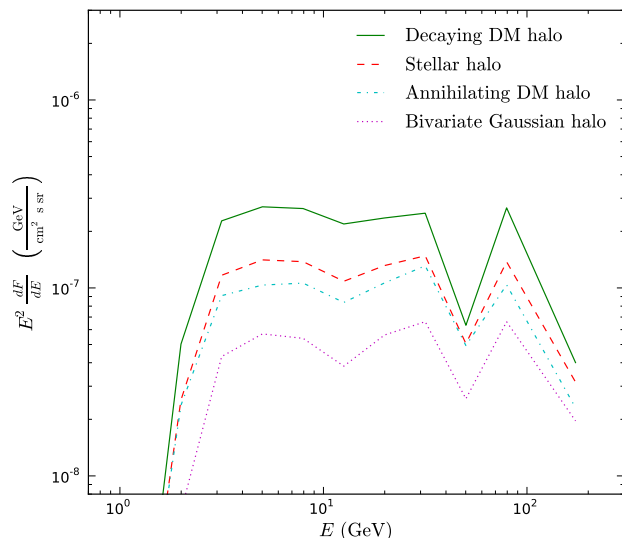### D. Different spherical profiles

FIG. 5: Best fit values of the flux associated with different spherical profiles. The values are found by fitting a three-template model (low energy bin, isotropic, and spherical templates) to the data. The case of NFW annihilation is discussed in details in Section III B.

In this section we compare different profiles with spherical symmetry. Together with the NFW DM annihilation profile $\propto \rho_{\mathrm{NFW}}^2$, studied in Section III B, we consider NFW DM decay $\propto \rho_{\mathrm{NFW}}$, a profile $\propto 1/r^3$ corresponding to the distribution of mass in stellar halo of Milky Way [20, 21] (r is the distance from the GC), and a bivariate gaussian profile with $\sigma_l = 15°$ and $\sigma_b = 25°$ studied in [18].

The best fit flux values associated with these profiles are shown in Figure 5. In Figure 6 we compare the χ^2 for these model with the null hypothesis (a low energy bin template plus an isotropic flux) from Section III B. We find that any of the spherical profiles give a significant improvement of χ^2 compared to the two-template model. The stellar halo profile has smaller χ^2 than the other three profiles. A possible astrophysical source of high energy gamma-rays at high latitudes could be a population of millisecond pulsars [22, 23].
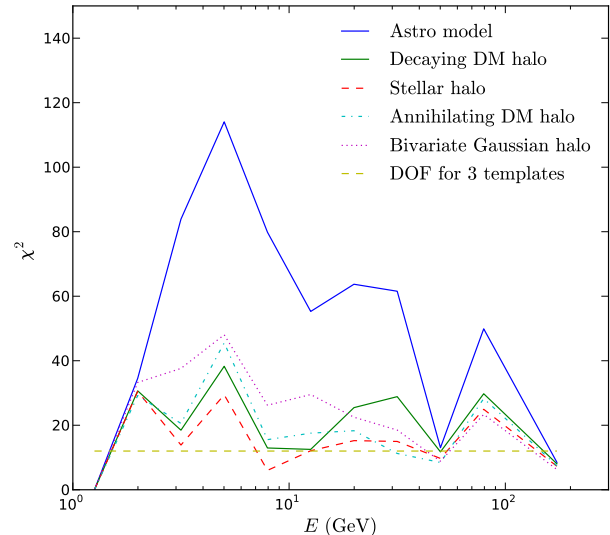

FIG. 6: Goodness of fit of the models presented in Figure 5 compared to the astrophysical model. The number of degrees of freedom (DOF) for the three-template model is thirteen (sixteen a_{l0} modes minus three parameters associated with the normalization of the templates).
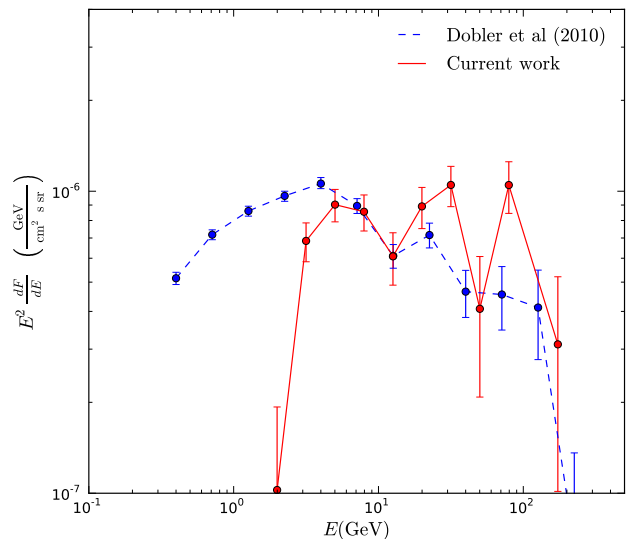
FIG. 7: Comparison with the gamma-ray haze spectrum in [18]. Our flux is the same as in Figure 5 but averaged over the window $l \in (-15°, 15°)$ and $b \in (-30°, -10°)$ [18].

In Figure 7 we compare our fit of the bivariate gaussian halo with the calculation in [18]. There is a general agreement above ~ 2 GeV. Our error bars are larger than the errors in [18], possibly, due to the usage of a subset of spherical modes with $m = 0$ rather than all spherical harmonics.

IV. ENERGY SPECTRUM

In this section we fit the fluxes found in the previous section by some general energy spectra. We assume that there are three main contributions to the gamma-ray flux: Galactic astrophysics emission, isotropic emission (extragalactic plus a possible contamination from misidentified cosmic rays), and an additional spherically symmetric flux. We fit the Galactic and the isotropic fluxes by power-law spectra. For the spherical template, we use a power-law with an exponential cutoff and an energy spectrum for DM annihilating into $b\bar{b}$.

A. Power-law energy spectra

In the previous section we have used a low energy bin as a template for the Galactic astrophysical component. In reality the flux in the first bin E_0 is a sum of all components. As a result there is a non-trivial relation between the fluxes associated to templates, and the intrinsic fluxes. Let us denote the intrinsic Galactic component of the flux by $\Phi_\mathrm{g}(E)$, the intrinsic isotropic component by $\Phi_\mathrm{i}(E)$, and a spherical ("dark matter") component by $\Phi_\mathrm{d}(E)$. The flux associated to the low energy bin will be denoted as $F_\mathrm{a}(E)$, the flux associated to isotropic template as $F_\mathrm{i}(E)$, and the flux associated to spherical templates as $F_\mathrm{d}(E)$.

The flux in the first energy bin is

$$F_\mathrm{a}(E_0) = \Phi_\mathrm{g}(E_0) + \Phi_\mathrm{i}(E_0) + \Phi_\mathrm{d}(E_0). \quad (9)$$

i.e., the corresponding template has contributions from the actual Galactic photons, from the isotropic distribution, and, possibly, from an additional spherical component. Consequently, a fraction of isotropic and DM photons is included in the flux corresponding to the "astrophysical" low energy bin template at all energy bins.

In this subsection, we consider the following parameterization of intrinsic fluxes

$$\Phi_\mathrm{g} = \Phi_\mathrm{g0} \left(\frac{E}{E_0} \right)^{-n_\mathrm{g}}, \quad (10)$$

$$\Phi_\mathrm{i} = \Phi_\mathrm{i0} \left(\frac{E}{E_0} \right)^{-n_\mathrm{i}}, \quad (11)$$

$$\Phi_\mathrm{d} = \Phi_\mathrm{d0} \left(\frac{E}{E_0} \right)^{-n_\mathrm{d}} e^{-\frac{E-E_0}{E_\mathrm{cut}}}. \quad (12)$$

If we assume that the Galactic gamma-rays provide the most significant contribution to the astro template at E_0, then we can expect that the astro template flux F_a has the same power-law index as the intrinsic Galactic flux Φ_g and the following parameterization of F_a is reasonable:

$$F_\mathrm{a}(E) = (\Phi_\mathrm{g0} + \Phi_\mathrm{i0} + \Phi_\mathrm{d0}) \left(\frac{E}{E_0} \right)^{-n_\mathrm{g}}. \quad (13)$$

The fluxes for the isotropic and DM templates are equal to the intrinsic fluxes minus the contribution to the "astro" template:

$$F_\mathrm{i}(E) = \Phi_\mathrm{i0} \left(\frac{E}{E_0} \right)^{-n_\mathrm{i}} - \Phi_\mathrm{i0} \left(\frac{E}{E_0} \right)^{-n_\mathrm{g}}, \quad (14)$$

$$F_\mathrm{d}(E) = \Phi_\mathrm{d0} \left(\frac{E}{E_0} \right)^{-n_\mathrm{d}} e^{-\frac{E-E_0}{E_\mathrm{cut}}} - \Phi_\mathrm{d0} \left(\frac{E}{E_0} \right)^{-n_\mathrm{g}} \quad (15)$$

In order to find the parameters of the energy spectra, we use the fluxes found in Section III B in every energy bin as "data points". The error bars are derived from Equations (13), (14), and (15). The models of the fluxes are parameterized in Equations (10), (11),(12). The best fit indices and the cutoff are presented in Table I.

The index $n_\mathrm{g} \approx 2.8$ for the Galactic component is consistent with the pion production of gamma-rays. The index $n_\mathrm{i} \approx 1.9$ for the isotropic flux is harder than the typical indices $n = 2.2-2.5$ for extragalactic diffuse background or AGN spectra [12, 24]. This discrepancy is most probably due to an isotropic energy dependent contamination from cosmic rays (CR). A model for the CR background in diffuse class events can be found in Figure 1 of Ref. [12]. The corresponding spectrum is rather hard, $\sim E^{-1}$, reaching $\sim O(1)$ fraction of the total flux around 100 GeV (compare Figure 1 and Table 1 in [12]).

Gamma-ray flux with an index $n_\mathrm{d} \approx 2$ can be obtained by inverse Compton scattering of interstellar radiation photons and a population of electrons with a spectrum $\sim E^{-3}$. A break at a few hundred GeV can be explained by transition between Thompson and Klein-Nishina scattering for star-light photons, $E_\mathrm{break} \sim (m_e c^2)^2/h\nu$. If we attribute the spherical signal with the ICS photons, then the question would be to find a spherically symmetric source of high energy electrons at high latitudes.

B. Limits on DM annihilation

In this subsection we use the flux associated with the NFW annihilation template derived in Section III B to put conservative upper limits on the rate of DM annihilation in the Milky Way halo. Assuming $b\bar{b}$ annihilation channel, we find the "best fit" DM mass and annihilation cross section. In the analysis, we use the prompt gamma-rays emitted by the decay of $b\bar{b}$, the corresponding spectrum is found with the help of the Pythia generator [25, 26]. The best fit DM parameters are subject to significant systematic uncertainties due to modeling of astrophysical emission. The upper limits, on the other hand, are rather robust. They only depend on DM profile and on annihilation channel, e.g., $b\bar{b}$, W^+W^- etc.

Let $\langle \sigma v \rangle$ denote the DM annihilation cross section. In this paper we will consider only the prompt gamma-ray emission from DM annihilation. The flux of gamma-rays from DM annihilation per steradian at an angle θ from

Model	n_{g}	n_{i}	n_{d}	E_{cut} (GeV)
Astro	2.62 ± 0.01	1.49 ± 0.03	–	–
Decay	2.79 ± 0.02	1.68 ± 0.04	2.13 ± 0.05	142
Annihilation	2.83 ± 0.02	1.88 ± 0.03	2.01 ± 0.05	137
Stellar halo	2.87 ± 0.02	1.89 ± 0.04	2.05 ± 0.05	152
Gaussian halo	2.84 ± 0.02	1.86 ± 0.04	1.98 ± 0.05	184

TABLE I: Fitting the fluxes associated with different templates by power-law intrinsic Galactic, isotropic, and spherically symmetric fluxes. The parameterization is given in Equations (13), (14), and (15). The profiles are defined in Section III D.
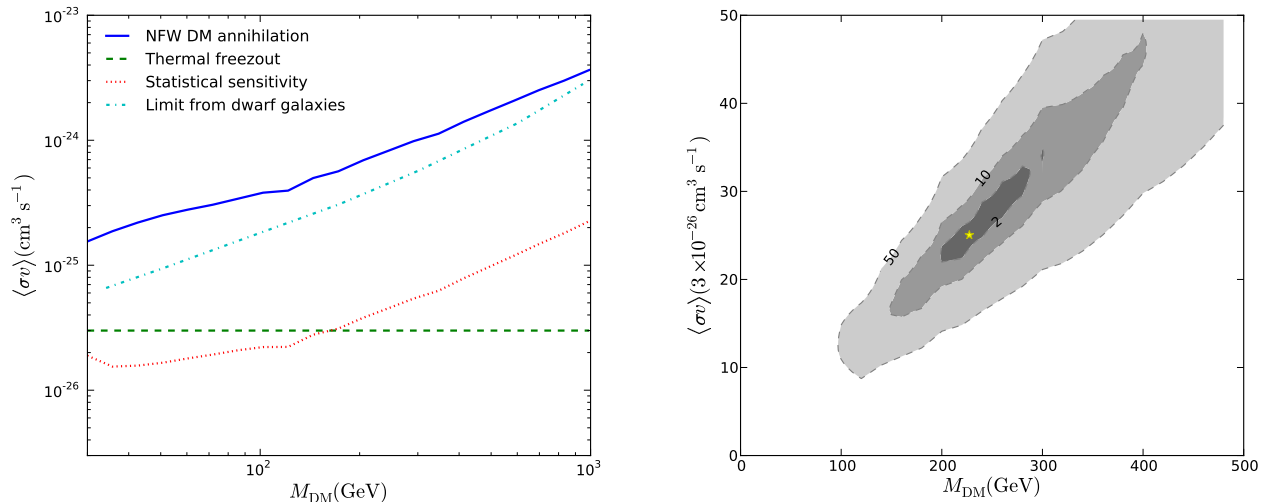

FIG. 8: Left plot: upper bound on DM $b\bar{b}$ annihilation in an NFW profile in comparison with the dwarf spheroidal galaxies limit [17]. The bound is derived by using the NFW annihilation flux in Figure 3 as an upper limit. The statistical sensitivity is derived from the error bars for NFW flux in Figure 3. Right plot: best $b\bar{b}$ DM annihilation fit to NFW flux points in Figure 3. Contours represent $\Delta\chi^2$. Limits from below are subject to systematic uncertainty due to modeling of astrophysical fluxes. Limits from above may depend slightly on DM profile and annihilation channel.

the GC is

$$F_{\mathrm{DM}}(E, \theta) = \frac{1}{8\pi} \frac{\langle \sigma v \rangle}{M_{\mathrm{DM}}^2} \frac{dN_\gamma}{dE} \int \rho_{\mathrm{DM}}^2(r) dR \qquad (16)$$

where $\frac{dN_\gamma}{dE}$ is an average spectrum of prompt gamma-rays per annihilation event, R is the distance along the line of sight, and r is the distance from GC, $r^2 = R^2 + R_0^2 + 2RR_0 \cos\theta$. We assume local DM density $\rho_{\mathrm{DM0}} = 0.4 \, \mathrm{GeV cm}^{-3}$ [27–29].

We parameterize the flux from DM annihilation by the DM mass and annihilation cross section. The result of fitting the corresponding energy density of the flux to the best fit fluxes associated with NFW annihilation template from Section III B is shown in Figure 8 on the right. There are significant systematic uncertainties, e.g., a distribution of inverse Compton photons, in proving an existence of DM annihilation signal. One can nevertheless put upper limits on DM annihilation, provided that the flux from DM cannot be larger than the signal correlated with the NFW annihilation template.

In Figure 8 on the left for every DM mass M_{DM} we find the best fit annihilation cross section which gives the upper limit on DM annihilation. Statistical uncertainty in

this case is an order of magnitude smaller than the limit itself. This uncertainty provides an estimate of statistical sensitivity of our method for the DM annihilation signal. For $M_{\mathrm{DM}} \lesssim 150$ GeV this sensitivity is sufficient to detect DM annihilating with freeze out cross section.

In spherical harmonics analysis the uncertainty is dominated by systematics while statistical uncertainty is rather small. This makes spherical harmonics a complimentary tool to the searches of DM annihilation in dwarf spheroidal galaxies [17, 30], where the systematic uncertainties are small and the limits are dominated by statistics.

V.   CONCLUSIONS

In this paper we argue that the spherical harmonics decomposition is a convenient tool to study the large scale distribution of gamma-rays such as a possible contribution from DM annihilation or decay. The key points of this approach are the use of the spherical harmonics decomposition in a window that eliminates most of the known astrophysical sources and the choice of the coordi-

nate system appropriate for the symmetries of DM distribution. In Appendix B we show that in a test with 10^4 randomly generated photons, a 4% fraction of gamma-rays coming from DM annihilation can be detected with a five sigma significance.

One of the main advantages of the spherical harmonics decomposition compared to the analysis in coordinate space is an efficient organization of the data. Consider, as an example, the top right plot in Figure 10. The harmonics with $\ell \lesssim 20$ are dominated by the large scale distribution of gamma-rays. The harmonics between $\ell \sim 20$ and $\ell \sim 200$ are dominated by the contribution from point sources, while the harmonics above $\ell \sim 200$ are dominated by the noise (either physical noise due to insufficient number of photons or the PSF of the instrument). Thus one can immediately separate the data that carry some information about the large scale distribution of gamma-rays from the harmonics dominated by the noise.

Another approach in finding DM signatures in gamma-rays actively discussed in the literature is to search for features in the power spectrum due to DM subhalos [31–33]. Our method is complimentary to this, since we look for the signature of the main halo at small ℓ, whereas DM subhalos usually contribute at $\ell \gtrsim 100$. We also believe that with the current volume of data our approach is more advantageous since $\ell \gtrsim 100$ harmonics are dominated by the noise and much more data will be necessary to separate a significant signal, whereas for small ℓ the current data is enough to overcome the noise level for energies up to $30 - 50$ GeV.

Our method already enables us to argue that there is a significant spherical distribution of photons in addition to an astrophysical flux, which we model by taking the data in a low energy bin as a template, plus an isotropic distribution of photons. We compare several profiles with a spherical symmetry around GC and find that below ~ 50 GeV "stellar" halo $\propto 1/r^3$ has a slightly better χ^2 than DM annihilation, DM decay, or a bivariate gaussian distribution found by [18].

We also use the flux associated with NFW annihilation template to put upper limits on DM annihilation into $b\bar{b}$. The derived limits are a factor of a few less stringent than the limits from dwarf spheroidal galaxies. The uncertainty of our method is dominated by systematics while the dSph method is dominated by statistics. One of the advantages of using the DM annihilation in the Milky Way halo versus the annihilation in dSph is the ability to use the *Fermi* data to put stronger constrains on DM annihilation, even after the *Fermi* LAT stops collecting data, by reducing the systematic uncertainty related to modeling the astrophysics backgrounds.

Appendix A: Spherical harmonics covariance

In this appendix we provide details on the calculation of covariance matrix for spherical harmonics defined in a window on the sphere.

Consider a pixelation of the sphere. We will assume that the pixel size is sufficiently small compared to the angular size of interest, but it is sufficiently large so that the photons in different pixels are uncorrelated. Denote by n_p the number of photons in a pixel p, let γ_p be the center of p, and $\delta\Omega_p$ be the area of p. We can define a discrete photon density function $\rho_p = \frac{n_p}{\delta\Omega_p}$. The spherical harmonics transform of the density function is

$$a_{lm} = \int Y_{lm}^*(\gamma)\rho(\gamma)d\Omega \approx \sum_{p=1}^{N_{\text{pix}}} Y_{lm}^*(\gamma_p)n_p, \qquad (A1)$$

The spherical functions are defined as

$$Y_{lm}(\theta,\varphi) = \sqrt{\frac{2l+1}{4\pi}\frac{(l-m)!}{(l+m)!}}P_l^m(\cos\theta)e^{im\varphi}. \qquad (A2)$$

The spherical harmonics are orthogonal on the sphere but on a window in the sphere they are not. As a result, we expect correlation between different harmonics.

The covariance matrix of a_{lm}'s is

$$\begin{aligned} C_{lm,\,l'm'} &= \langle a_{lm}^* a_{l'm'}\rangle - \langle a_{lm}^*\rangle\langle a_{l'm'}\rangle \qquad (A3) \\ &= \sum_p Y_{l'm'}^*(\gamma_p)Y_{lm}(\gamma_p)(\langle n_p^2\rangle - \langle n_p\rangle^2), \end{aligned}$$

where we have used that the numbers of photons at different points are not correlated $\langle n_p n_{p'}\rangle = \langle n_p\rangle\langle n_{p'}\rangle$.

For a Poisson distribution $\langle n_p^2\rangle - \langle n_p\rangle^2 = \langle n_p\rangle$. In a particular realization of the photon map, our best estimate of $\langle n_p\rangle$ is the actual number of photons in this pixel n_p. Consequently, the covariance matrix can be estimated as

$$C_{lm,\,l'm'} = \sum_p Y_{l'm'}^*(\gamma_p)Y_{lm}(\gamma_p)n_p. \qquad (A4)$$

Spherical harmonics coefficients a_{lm} together with their covariance matrix provide the data necessary to formulate a χ^2 fitting procedure. Denote by $b_{lm}(\alpha)$ the spherical harmonics decomposition of a model prediction for the distribution of gamma-rays depending on a set α of parameters describing the model. The best fit parameters can be found by minimizing

$$\chi^2(\alpha) = \sum_{lm,\,l'm'} C_{lm,\,l'm'}^{-1}(a_{lm}^* - b_{lm}^*(\alpha))(a_{l'm'} - b_{l'm'}(\alpha)),$$
$$(A5)$$

where the star denotes complex conjugate and $C_{lm,\,l'm'}^{-1}$ is the inverse of the covariance matrix

$$\sum_{l'm'} C_{lm,\,l'm'}^{-1}C_{l'm',\,l''m''} = \delta_{ll''}\delta_{mm''}. \qquad (A6)$$

Appendix B: Monte Carlo test

In this appendix we check our method for separating a DM fraction by generating random distributions of photons. For the test we use an isotropic distribution plus
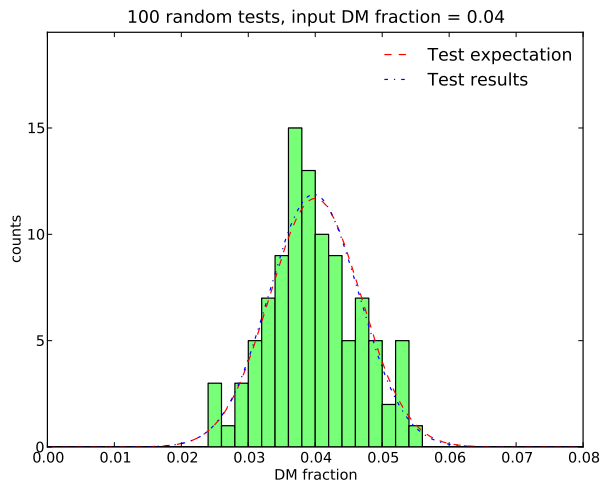
FIG. 9: Random test of the spherical harmonics decomposition algorithm for separating a DM NFW annihilation signal from an isotropic background. The input DM fraction is 0.04. Plotted fractions represent the result of fitting in spherical harmonics space. An approximation of these fractions by a gaussian distribution is the "Test results" curve. "Test expectation" is a gaussian around 0.04 with the scatter derived from Equation (7).

a distribution coming from DM annihilation in an NFW profile (Equation (8)).

The model parameters are the same as in Section III A: the window is $|b| > 10°$; we use Y_{lm} harmonics with $l = 0, \dots, 15$ and $m = 0$; the HEALPix parameter is nside = 32.

The average total number of photons inside the window is 10^4 with an average fraction of photons coming from DM annihilation 0.04. In every pixel p we put a random number of photons n_p according to the Poisson distribution with an average equal to the combined density at that pixel $\mu_p = \mu_p^{\text{isotr}} + \mu_p^{\text{DM}}$.

In the test we generated $N_{\text{tests}} = 100$ realizations of the photon map. For every realization i, we find the best estimate of the DM fraction q_i^{DM}. The average among the realization and the standard deviation are $(3.98 \pm 0.67) \times 10^{-2}$. The corresponding distribution is presented in Figure 9 as "test results".

In real applications, there is usually only one realization of the data available, i.e., we need a way to estimate the uncertainty of the result based only on one realization. This uncertainty can be estimated from the curvature of χ^2 near the minimum in the direction of the parameter (Equation (7)). The uncertainty derived from χ^2 (averaged over the realizations) is $\sigma = 0.68 \times 10^{-2}$. The corresponding Gaussian distribution $(4.00 \pm 0.68) \times 10^{-2}$ is plotted in Figure 9 as "test expectation".

The expected deviation of the mean is $\sigma/\sqrt{N_{\text{tests}}} \approx 0.07$. Thus the actual deviation of the mean DM fraction from the expected value is less than one sigma. Also the difference of the actual standard deviation and the expected one is less than one sigma. We conclude that,

given a particular distribution of photons, the best estimate of the variance given by Equation (7) is an adequate representation of the actual variance among the realizations of the photon distribution.

The $\chi^2 = 13.9 \pm 5.2$ is calculated from Equation (A5). The number of degrees of freedom is fourteen: there are sixteen data points corresponding to Y_{l0} harmonics for $l = 0, \dots, 15$ and two varying parameters corresponding to the normalization of the two templates: isotropic and DM.

We find that the spherical harmonics decomposition is a statistically unbiased fitting method with a viable estimation of statistical uncertainty.

Appendix C: Point sources

In this appendix we study the dependence of spherical harmonics on the contribution from point sources. We find that in the presence of point sources the variance of a_{lm}'s increases.

We will assume some pixelation of the sphere with pixels of equal area. Denote by n_p the number of photons in a pixel p and define the spherical harmonics coefficients

$$a_{lm} = \sqrt{\frac{4\pi}{N_\gamma}} \sum_p Y_{lm}^*(\gamma_p) n_p \qquad \text{(C1)}$$

where the sum is over the pixels, γ_p is the center of pixel p, N_γ is the total number of photons. The normalization of a_{lm}'s in this appendix is different from the normalization everywhere else in the paper. We show below that with this normalization the expected variance of spherical harmonics in the case of Poisson noise is equal to one.

Analogously to the derivation of the covariance matrix in Equation (A3), we find that the variance of a_{lm}'s is

$$\text{Var}(a_{lm}) = \frac{4\pi}{N_\gamma} \sum_p Y_{lm}^*(\gamma_p) Y_{lm}(\gamma_p) \text{Var}(n_p) \qquad \text{(C2)}$$

If we assume that the diffuse emission and the point sources were distributed isotropically, then $\langle a_{lm} \rangle = 0$ and $\langle a_{lm}^2 \rangle = \langle a_{lm'}^2 \rangle$ for any l, m, m'. In this case, one can relate the variance of spherical harmonics to the expectation value of the angular power spectrum

$$\text{Var}(a_{lm}) = \frac{1}{2l+1} \sum_{m=-l}^{l} \text{Var}(a_{lm}) = \langle C_l \rangle. \qquad \text{(C3)}$$

In the following we will show that this is a good approximation for large ℓ, whereas small ℓ harmonics are dominated by the non-isotropic Galactic emission with $\langle a_{lm} \rangle \neq 0$.

In the case of the Poisson statistics, the best estimate for the variance of the number of photons is $\text{Var}(n_p) = n_p$. Taking into account that for any point on the sphere

$$\frac{1}{2l+1} \sum_m Y_{lm}^*(\gamma) Y_{lm}(\gamma) = \frac{1}{4\pi} \qquad \text{(C4)}$$

we find from Equations (C2 - C4) that in the case of the Poisson noise

$$\text{Var}(a_{lm}) = \frac{1}{N_\gamma} \sum_p \text{Var}(n_p) = 1 \qquad (C5)$$

Now suppose that there are some point sources. Denote by x_m the expected number of m-photon sources inside a pixel. In this case the statistics of photons in pixels across the sky is not Poisson. Instead, we will assume the Poisson statistics of the point sources with the average values x_m. In particular the variance of the number of photon sources is

$$\text{Var}(x_m) = x_m \qquad (C6)$$

The variance of the number of photons in a pixel is the sum of the variances of the photon sources times the number of photons from every source squared

$$\text{Var}(n_p) = \sum_m m^2 \text{Var}(x_m) = \sum_m m^2 x_m \qquad (C7)$$

Let us introduce the following parameter

$$m_{\text{av}} = \frac{\sum_m m^2 x_m}{\sum_m m x_m}, \qquad (C8)$$

where $\sum_m m x_m = \langle n_p \rangle$ is the expected number of photons in a pixel. If there is a significant contribution of multi-photon point sources to gamma-ray data, then $m_{\text{av}} \gg 1$, while $m_{\text{av}} = 1$ for truly diffuse emission. In analogy with Equation (C5), we find

$$\text{Var}(a_{lm}) = \frac{1}{N_\gamma} \sum_p \text{Var}(n_p) = m_{\text{av}} \qquad (C9)$$

To summarize, for isotropic distribution of photons and for for the angular scales smaller than the detector PSF, we expect

$$\langle C_l \rangle = 1. \qquad (C10)$$

This limit should be saturated for sufficiently large ℓ.

In the presence of point sources, the variance is m_{av} times larger than the variance in the Poisson statistics case. Consequently, for isotropic distribution of point sources (or when the angular scale corresponding to ℓ is much smaller than the scale of the distribution), we expect

$$\langle C_l \rangle = m_{\text{av}}. \qquad (C11)$$

We expect this behavior for intermediate values of ℓ. At small ℓ, the C_l's are dominated by a large scale distribution of gamma-rays.

In Figure 10 we compare the angular power spectra before and after masking the gamma-ray point sources for several characteristic energy bins. We use the same *Fermi* data as described in Section III A and mask the Galactic plane within $|b| < 10°$. For $\ell \lesssim 20$ the angular power spectrum is dominated by the large scale distribution of photons: these values of ℓ are of interest for fitting templates at large angular scales using the spherical harmonics. For intermediate ℓ's the angular power spectrum is dominated by the contribution from point sources. For large ℓ the angular power spectrum is consistent with the Poisson noise with an exception of the highest energy bin (100 GeV - 300 GeV), where the the signal in the presence of point sources is above the Poisson noise level even for $\ell \sim 1000$ corresponding to angular scales $\sim 0.2°$. This is consistent with the PSF $\lesssim 0.1°$ for gamma-rays with energies above 100 GeV [11].

In the analysis we use the HEALPix parameter nside = 1024 which corresponds to approximately 10^7 pixels. The "pixelized" values of C_l's are supposed to be smaller than the values computed by a continuous integration, $C_{l \, \text{pix}} = w_l^2 C_{l \, \text{cont}}$, where w_l is the pixel window function. The window function is a decreasing function which is equal to 1 at $\ell = 0$. For nside = 1024 and $\ell = 1000$, $w_l^2 \approx 0.956$, i.e. the values of C_l's in Figure 10 are less than about 5% smaller than the real values. For nside = 32 the window function at $\ell = 15$ is $w_l = 0.989$. We didn't rescale the spherical harmonics by the window function in the fitting procedure. The only effect of the window function is to put a little more weight on lower harmonics.

Let us make one more technical comment about the derivation of the plots in Figure 10. In order to relate the variance in the spherical harmonics to the value of C_l's we need the average $\langle a_{lm} \rangle = 0$. In the analysis we have used the spherical harmonics decomposition in a window $|b| > 10°$ (the window is the same as defined in section III A). For the spherical harmonics decomposition in a window, at least some of the expected a_{lm}'s are non-zero. In order to make them zero without affecting the variance we subtract the spherical harmonics of an isotropic distribution inside the window.

[1] Y. B. Zeldovich, A. A. Klypin, M. Y. Khlopov, and V. M. Chechetkin, Sov. J. Nucl. Phys. **31**, 664 (1980).

[2] V. Springel *et al.*, Nature (London) **456**, 73 (2008),

arXiv:0809.0894.

[3] J. M. Siegal-Gaskins and V. Pavlidou, PRL **102**, 241301 (2009), arXiv:0901.3776.

[4] J. F. Navarro, C. S. Frenk, and S. D. M. White, Astrophys. J. **490**, 493 (1997), arXiv:astro-ph/9611107.

[5] J. Diemand *et al.*, Nature (London) **454**, 735 (2008), arXiv:0805.1244.

[6] M. Kuhlen, J. Diemand, and P. Madau, Astrophys. J. **686**, 262 (2008), arXiv:0805.4416.

[7] V. Springel *et al.*, Mon. Not. R. Astron. Soc. **391**, 1685 (2008), arXiv:0809.0898.

[8] F. K. Hansen, K. M. Górski, and E. Hivon, Mon. Not. R. Astron. Soc. **336**, 1304 (2002), arXiv:astro-ph/0207464.

[9] K. M. Górski *et al.*, Astrophys. J. **622**, 759 (2005), arXiv:astro-ph/0409513.

[10] A. A. Abdo *et al.*, Astrophys. J. **188**, 405 (2010), arXiv:1002.2280.

[11] W. B. Atwood *et al.*, Astrophys. J. **697**, 1071 (2009), arXiv:0902.1089.

[12] A. A. Abdo *et al.*, Physical Review Letters **104**, 101101 (2010), arXiv:1002.3603.

[13] M. C. Smith *et al.*, Mon. Not. R. Astron. Soc. **379**, 755 (2007), arXiv:astro-ph/0611671.

[14] X. X. Xue *et al.*, Astrophys. J. **684**, 1143 (2008), arXiv:0801.1232.

[15] J. F. Navarro *et al.*, Mon. Not. Roy. Astron. Soc. **349**, 1039 (2004), arXiv:astro-ph/0311231.

[16] A. A. Abdo *et al.*, PRL **104**, 091302 (2010), arXiv:1001.4836.

[17] A. A. Abdo *et al.*, Astrophys. J. **712**, 147 (2010), arXiv:1001.4531.

[18] G. Dobler, D. P. Finkbeiner, I. Cholis, T. Slatyer, and N. Weiner, Astrophys. J. **717**, 825 (2010), arXiv:0910.4583.

[19] M. Su, T. R. Slatyer, and D. P. Finkbeiner, Astrophys. J. **724**, 1044 (2010), arXiv:1005.5480.

[20] E. F. Bell *et al.*, Astrophys. J. **680**, 295 (2008), arXiv:0706.0004.

[21] M. Jurić *et al.*, Astrophys. J. **673**, 864 (2008), arXiv:astro-ph/0510520.

[22] C. Faucher-Giguère and A. Loeb, Journal of Cosmology and Astro-Particle Physics **1**, 5 (2010), arXiv:0904.3102.

[23] D. Malyshev, I. Cholis, and J. D. Gelfand, arXiv:1002.0587 (2010), arXiv:1002.0587.

[24] A. A. Abdo *et al.*, Astrophys. J. **720**, 435 (2010), arXiv:1003.0895.

[25] T. Sjöstrand, S. Mrenna, and P. Skands, Journal of High Energy Physics **5**, 26 (2006), arXiv:hep-ph/0603175.

[26] T. Sjöstrand, S. Mrenna, and P. Skands, Computer Physics Communications **178**, 852 (2008), arXiv:0710.3820.

[27] R. Catena and P. Ullio, arXiv:0907.0018 (2009), arXiv:0907.0018.

[28] M. Weber and W. de Boer, Astron. Astrophys. **509**, A25 (2010), arXiv:0910.4272.

[29] P. Salucci, F. Nesti, G. Gentile, and C. F. Martins, ArXiv:1003.3101 (2010), arXiv:1003.3101.

[30] M. Llena Garde, ArXiv:1102.5701 (2011), arXiv:1102.5701.

[31] S. Ando, Phys. Rev. D **80**, 023520 (2009), arXiv:0903.4685.

[32] B. S. Hensley, J. M. Siegal-Gaskins, and V. Pavlidou, arXiv:0912.1854 (2009), arXiv:0912.1854.

[33] A. Cuoco, A. Sellerholm, J. Conrad, and S. Hannestad, arXiv:1005.0843 (2010), arXiv:1005.0843.

[34] `http://code.google.com/p/healpy/`, `http://healpix.jpl.nasa.gov`.

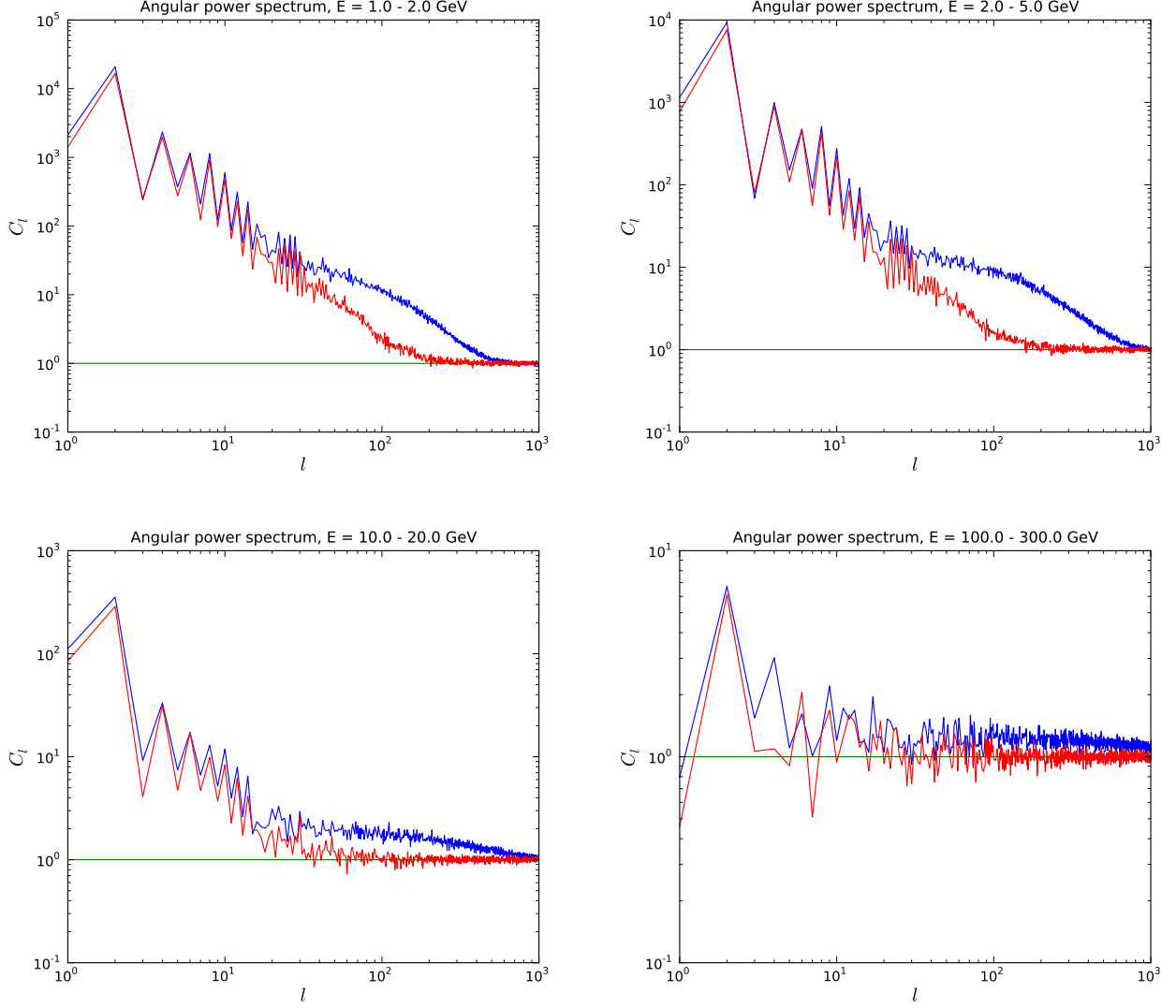[35] The *Fermi* background emission model can be found at `http://fermi.gsfc.nasa.gov/ssc/data/access/lat/`

FIG. 10: Power spectrum of angular modes for *Fermi* gamma-ray data inside a window excluding the Galactic plane $|b| > 10°$ for some characteristic energy bins. Blue lines (upper): all gamma-rays are taken into account, including point sources. Red lines (lower): *Fermi* gamma-ray point sources [10] are masked. The normalization is chosen such that $\langle C_l \rangle = 1$ for the Poisson noise (green constant lines). At low ℓ the power spectrum is dominated by the large scale structure (the red and the blue curves are almost identical). At $\ell \sim 100$ the C_l's are dominated by the point sources (the blue curve is significantly higher than the red curve). For zero PSF, the blue curve would stay for large ℓ at a constant level, given by Equation C11, above the Poisson noise level. The suppression of C_l's to the Poisson noise level for higher ℓ is due to non-zero PSF. In the highest energy bin, 100 - 300 GeV, the PSF is less than 0.1° [11] which corresponds to $\ell > 2000$. As a result, the blue curve stays above the red curve in this energy bin. At lower energies the PSF is higher and the suppression of the angular power spectrum to the Poisson noise level occurs for smaller ℓ's. In the plots, we use the HEALPix parameter nside = 1024.